Elsevier Editorial System(tm) for Journal of Power Sources
Manuscript Draft

Manuscript Number: POWER-D-15-03781

Title: Synthetic approach from polypyrrole nanotubes to nitrogen doped pyrolyzed carbon nanotubes for asymmetric supercapacitors

Article Type: Research Paper

Keywords: Polypyrrole, N doped carbon, Nanotubes, Asymmetric supercapacitors

Corresponding Author: Dr. Deepak Dubal, M.Sc.Ph.D.

Corresponding Author's Institution: Catalan Institute of Nanoescience and Nanotechnology

First Author: Deepak Dubal, M.Sc.Ph.D.

Order of Authors: Deepak Dubal, M.Sc.Ph.D.; Nilesh Chodankar; Zahilia Caban-Huertas; Franciele Wolfart; Marcio Vidotti; Rudolf Holze; Chandrakant D Lokhande; Pedro Gomez-Romero

Manuscript Region of Origin: SPAIN

Abstract: Pseudocapacitive materials are highly capable to achieve high energy density integrated with high power electrostatic capacitive materials. However, finding a suitable electrostatic capacitive material to integrate with pseudocapacitive material in order to achieve high energy density with good rate capability is still a challenge. Herein, we are providing a novel synthetic approach starting from the synthesis of polypyrrole nanotubes (PPy-NTs) and ending up at the carbonization of PPy-NTs to obtain N-doped carbon nanotubes (N-CNTs). With highly porous nature of PPy-NTs and great graphitic texture with copious heteroatom functionalities, N-CNTs significantly promoted the faradic pseudo-capacitors, demonstrating high single-electrode capacitance over 332 F/g(PPy-NTs) and 228 F/g(N-CNTs) in 1 M H2SO4 aqueous solution. Further, a novel asymmetric supercapacitor with PPy-NTs as positive and N-CNTs as negative electrode has been fabricated. This PPy-NTs//N-CNTs cell effectively provides high operation voltage (1.4 V) and hence high energy density over 28.95 Wh/kg (0.41 mWh/cm3) with a high power density of 7.75 kW/kg (113 mW/cm3) and cyclic stability of 89.98 % after 2000 cycles.

Date: 4 August 2015

To

The Editor

Journal of Power Sources

Dear Editor,

This investigation accompanies the online submission of our new article entitled **"Synthetic approach from polypyrrole nanotubes to nitrogen doped pyrolyzed carbon nanotubes for asymmetric supercapacitors"** by *Deepak P. Dubal*, Nilesh R. Chodankar, Zahilia Caban-Huertas, Franciele Wolfart, Marcio Vidotti, Rudolf Holze, Chandrakant D. Lokhande, Pedro Gomez-Romero* for publication in ***Journal of Power Sources***

Pseudocapacitive materials are highly capable to achieve high energy density integrated with high power electrostatic capacitive materials. However, finding a suitable electrostatic capacitive material to integrate with pseudocapacitive material in order to achieve high energy density with good rate capability is still a challenge. Herein, we are providing a novel synthetic approach starting from the synthesis of polypyrrole nanotubes (PPy-NTs) and ending up at the carbonization of PPy-NTs to obtain N-doped carbon nanotubes (N-CNTs). With highly porous nature of PPy-NTs and great graphitic texture with copious heteroatom functionalities, N-CNTs significantly promoted the faradic pseudo-capacitors, demonstrating high single-electrode capacitance over 332 $F/g_{(PPy\text{-}NTs)}$ and 228 $F/g_{(N\text{-}CNTs)}$ in 1 M H_2SO_4 aqueous solution. Further, a novel asymmetric supercapacitor with PPy-NTs as positive and N-CNTs as

negative electrode has been fabricated. This PPy-NTs//N-CNTs cell effectively provides high operation voltage (1.4 V) and hence high energy density over 28.95 Wh/kg (0.41 mWh/cm^3) with a high power density of 7.75 kW/kg (113 mW/cm^3) and cyclic stability of 89.98 % after 2000 cycles.

The work has not been submitted previously to the Journal of Power Sources (in part or in whole), that it has not been published previously (except as an abstract, part of published lecture, or academic thesis), is not under consideration for publication elsewhere, and is approved by all authors and host authorities.

Please feel free to contact us for further information

Yours Sincerely,

Dr. Deepak P. Dubal, Ph. D.

Marie-Curie Fellow (BP-DGR), (Alexander von Humboldt Fellow, Germany)

Catalan Institute of Nanoscience and Nanotechnology, CIN2, ICN2 (CSIC-ICN)

Campus UAB, E-08193 Bellaterra (Barcelona), Spain

Research Highlights

- Synthesis of 1D PPy nanotubes
- Carbonization of PPy nanotubes to prepare N doped carbon nanotubes (N-CNTs)
- Fabrication of asymmetric supercapacitor with PPy-NTs//N-CNTs
- High performance asymmetric device

Synthetic approach from polypyrrole nanotubes to nitrogen doped pyrolyzed carbon nanotubes for asymmetric supercapacitors

Deepak P. Dubal [1], Nilesh R. Chodankar [2], Zahilia Caban-Huertas [1], Franciele Wolfart,[3] Marcio Vidotti,[3] Rudolf Holze [4], Chandrakant D. Lokhande [2], Pedro Gomez-Romero [1]***

[1]Catalan Institute of Nanoscience and Nanotechnology, CIN2, ICN2 (CSIC-ICN), Campus UAB, E-08193 Bellaterra, Barcelona, Spain

[2]Thin Film Physics Laboratory, Department of Physics, Shivaji University, Kolhapur, - 416004 (M.S), India

[3]Grupo de Pesquisa em Macromoléculas e Interfaces, Departamento de Química, Universidade Federal do Paraná, CP 19081, 81531-980, Curitiba, PR, Brazil

[4]Technische Universität Chemnitz, Institut für Chemie, AG Elektrochemie, D-09107 Chemnitz, Germany

CORRESPONDING AUTHOR FOOTNOTE

Dr. Deepak Dubal and Prof. Pedro Gomez-Romero

Tel.: +349373609/+345929950 Fax: +345929951

E-mail: dubaldeepak2@gmail.com (D. Dubal),

pedro.gomez@cin2.es (P. Gomez-Romero)

Abstract

Pseudocapacitive materials are highly capable to achieve high energy density integrated with high power electrostatic capacitive materials. However, finding a suitable electrostatic capacitive material to integrate with pseudocapacitive material in order to achieve high energy density with good rate capability is still a challenge. Herein, we are providing a novel synthetic approach starting from the synthesis of polypyrrole nanotubes (PPy-NTs) and ending up at the carbonization of PPy-NTs to obtain N-doped carbon nanotubes (N-CNTs). With highly porous nature of PPy-NTs and great graphitic texture with copious heteroatom functionalities, N-CNTs significantly promoted the faradic pseudo-capacitors, demonstrating high single-electrode capacitance over 332 $F/g_{(PPy\text{-}NTs)}$ and 228 $F/g_{(N\text{-}CNTs)}$ in 1 M H_2SO_4 aqueous solution. Further, a novel asymmetric supercapacitor with PPy-NTs as positive and N-CNTs as negative electrode has been fabricated. This PPy-NTs//N-CNTs cell effectively provides high operation voltage (1.4 V) and hence high energy density over 28.95 Wh/kg (0.41 mWh/cm^3) with a high power density of 7.75 kW/kg (113 mW/cm^3) and cyclic stability of 89.98 % after 2000 cycles.

Introduction

Supercapacitors with exclusive advantages over lithium ion batteries such as high power density and long cycling life are emerging as attractive electrochemical energy storage devices for various applications [1]. However, low energy density of supercapacitors hinders their practical applications. Intensive efforts have been dedicated to enhance their energy density to make it comparable to that of Li-ion batteries. Among supercapacitor electrode materials, pseudocapacitive transition-metal oxides (MnO_2, IrO_2, RuO_2 etc.), polyoxometalates and electronically conducting polymers (polyaniline, polypyrrole etc.) based on faradic redox charge storage have attracted significant attention because of their higher energy density than those of electrical double-layer capacitive carbon materials [2].

Recently, there are two promising and effective approaches are commonly adopted to improve the energy density of supercapacitors according to the equation ($E=0.5\ CV^2$), one is increasing the capacitance of device which is possible by fabricating different nanostructures (including, 0D, 1D, 2D and 3D) of the electrode materials [3]. Nanostructured electrodes provide high surface area, low diffusion paths and easy intercalation/de-intercalation of electrolyte ions which consequently improves the electrochemically active surface area [4]. Later possible way to improve energy density is extending operational voltage window of device which can be possible by using organic/ionic liquid electrolytes that are operated at higher voltages. However, their toxicity and high costs restrict their commercial applications. Recent, most interesting and successful way to extend the operational voltage window is assembly of asymmetric supercapacitors with aqueous electrolyte [5]. Asymmetric supercapacitor is configured by using pseudo-capacitive (faradaic) material as positive with non-faradaic material as negative electrodes in single cell to extend working potential window. Several probable and prosperous examples are presented in the literature [6]. The key to achieve high operational voltage is pairing of pseudocapacitive material with suitable capacitive material in order to achieve high energy density with good rate capability [7].

Our present investigation provides a novel strategy to fabricate asymmetric supercapacitor where 1D nanostructured conducting polymer (herein, polypyrrole nanotubes (PPy-NTs)) is used as positive electrode; furthermore these PPy-NTs were carbonized in nitrogen atmosphere to obtain N-CNTs and used as negative electrode. Compared to solid nanostructures (e.g. nanowires), tubular nanostructures typically offer higher surface area with less utilization of mass, resulting in more gravimetric specific capacitance. Moreover, the longitudinal axis of 1D nanostructure can provide efficient transport pathway for both electrons and ions. Thus, we can take an advantage of tubular structure in both electrodes. In addition, the introduction of foreign atoms such as boron, phosphorus and especially nitrogen significantly affect chemical, mechanical, and electronic properties of carbon materials. As an electrode material, the nitrogen doped carbon materials exhibit excellent electrochemical properties such as high specific capacitance (250-400 F/g), excellent rate capability and fair large potential window [8].

Herein, 1D PPy nanotubes (PPy-NTs) are synthesized through chemical oxidation mediated soft template-directed route using anions azo dye methyl orange (MO). Later, as-prepared PPy-NTs were carbonized at 800 °C under nitrogen in order to obtain N doped carbon nanotubes (N-CNT). The electrochemical supercapacitive properties of PPy-NTs and N-CNTs have been investigated with 3-electrode configuration in 1 M H_2SO_4 electrolyte. Further, an asymmetric supercapacitor is devised with PPy-NTs as positive and N-CNTs as negative electrodes. Thanks to the integration of pseudocapacitors (PPy-NTs) and EDLCs (N-CNTs) at both ends, the PPy-NTs//N-CNTs could realize a broad voltage of 1.4 V and amazingly attain a remarkable energy density of 28.95 Wh/kg.

Experimental

Synthesis of PPy-NTs and N-CNTs

Briefly, 5 mM MO (sodium 4-[40 (dimethylamino)phenyldiazo]phenylsulfonate ($(CH_3)_2NC_6H_4$-N=$NC_6H_4SO_3Na$) and 1.5 mM $FeCl_3$ (0.243 g) were dissolved in 30 ml double

distilled water (DDW) which will turn in a flocculent precipitate immediately. In the next step, 0.1 mL (1.5 mM) pyrrole monomer was added above solution and the mixture was stirred at room temperature for 24 h. After 24 h, the formed precipitate was filtered and repeatedly washed with mixture of DDW and ethanol to get neutral pH and finally the filtered product was dried overnight under vacuum at 333 K.

In order to prepare N doped carbon nanotubes (N-CNTs), above prepared PPy-NTs were subjected to carbonization at 800 °C for 1 h, with a heating rate of 5 °C/min under N_2 atmosphere.

Material Characterization

The surface morphology of as-prepared PPy-NTs and N-CNTs samples were investigated using the field-emission scanning electron microscopy (FEI Quanta 650F Environmental SEM) attached with an energy-dispersive X-ray spectroscopy (EDS) analyzer to measure the sample composition and transmission electron microscopy (Tecnai G2 F20 S-TWIN HR(S) TEM, FEI). Powder X-ray diffraction study was performed using Panalytical X'pert Pro-MRD instrument (Cu $K_{\square}$ radiation and PIXel detector). The X-ray photoelectron spectra (XPS) analyses were obtained by X-ray photoelectron spectroscopy (XPS, SPECS Germany, PHOIBOS 150). N_2 adsorption/desorption was determined by Brunauer-Emmett-Teller (BET) measurements using Micromeritics instrument (Data Master V4.00Q, Serial#:2000/2400).

Electrochemical measurements

To measure the electrochemical features, 85 % of active material (PPy-NTs or N-CNTs) was mixed with 10 % PVDF as binder and 5 % acetylene black. Further the few drops of NMP (solvent) were added in mixture and crushed using mortar to get uniform paste. Finally the paste was applied on commercial flexible carbon cloth which further used as SCs electrodes. The electrochemical properties were measured using standards three electrode system which contain working electrode (PPy-NTs or N-CNTs), counter electrode (platinum) and reference electrode (Ag/AgCl) in 1M H_2SO_4 electrolyte. Later, the asymmetric cell was fabricated using

PPy-NTs as a positive and N-CNTs as negative electrode with 1 M H_2SO_4 electrolyte. The all electrochemical measurements were carried out using the cyclic voltammetry (CV), galvanostatic charge-discharge with Biologic VMP3 potentiostat.

Result and discussion

The X-ray diffraction patterns of as-prepared PPy-NTs and N-CNTs are presented in Fig. 1 (a). As seen in Fig. 1 (a), both PPy-NTs and N-CNTs exhibit amorphous nature. It is interesting to note that, for PPy-NTs, a broad hump is observed, corresponding to the repeat unit of pyrrole ring in PPy, implying the polymer chain is highly oriented [9]. While in case of N-CNTs, peak intensity is considerably decreased with slight shifting toward lower angles site (25.5°) showing highly graphitic texture. The amorphous materials are demanded for energy storage devices as it draw easy route for intercalation/deintercalation of electrolyte ions during electrochemical reactions [10]. Later, in order to get more insights about elements and oxidation states of the as-prepared PPy-NTs and N-CNTs, XPS analysis was performed and the corresponding results are presented in Fig. 1 (b-d). Fig. 1 (b) reveals the wide scan spectra of PPy-NTs and N-CNTs, showing presence of characteristics C1s**,** N1s and O1s peaks. The intensities of N1s and O1s peaks are reduced with predominant increase in C1s peak for N-CNTs sample as compared to PPy-NTs confirming the expected conversion after carbonization. As the conducting polymers are nitrogen containing aromatic polymer materials, PPy-NTs possesses N1s peak. The oxygen has probably originated from the surface oxidation of PPy-NTs/N-CNTs [11]. The narrow scan spectrum of C1s for N-CNTs is presented in Fig. 1 (c), which can be primarily fitted as three peaks centered at binding energies of 284.6, 285.5 and 287.7 eV. In detail, the peak at the binding energy of 284.6 eV confirms the presence of graphitic carbon, corresponding to the energy of sp^2 C=C bond in C1s spectrum of pyrolytic graphite. Further the small signals at higher binding energies corresponds to C-O (285.5 eV) and C-N (287.7 eV) species in N-CNTs, respectively [12]. It is imperative to confirm the

oxidation states of nitrogen in PPy-NTs and N-CNTs for the final approval of expected material formation. Fig. 1 (d) shows the narrow scan spectra of N1s for PPy-NTs and N-CNTs. Interestingly, PPy-NTs consist of single peak at 399.7 eV, which is characteristic peak of neutral nitrogen in PPy ring (-NH-) and designated as 'pyrrolic' nitrogen [9]. While, for N-CNTs, two distinct peaks at 398.2 and 400.9 eV are clearly observed. Among them, the peak with binding energy 398.2 eV corresponds to the 'pyridinic' nitrogen while peak at 400.9 eV attributed to the 'graphitic' nitrogen. Thus, the peak at 398.2 eV is contributing to the π-conjugated system with a pair of p-electrons whereas that at 400.9 eV is observed only when the carbon atoms are substituted by the nitrogen to form the 'graphitic' nitrogen [13]. Ultimately, with XPS analysis, it is clear that the nitrogen present in PPy-NTs and N-CNTs is in different oxidation states confirming the formation of nitrogen doped CNTs (N-CNTs). The graphitic N doped inside the aromatic ring (quaternary N) creates a positive charge properties and electron acceptor, which enhance the conductivity of carbon material. Besides, these heteroatoms doped into carbon networks render more internal surfaces ion-accessible by strengthening wettability of electrolyte-electrode interface.

Raman spectra of PPy-NTs and N-CNTs are demonstrated in Fig. 2 (a, b). The peaks at 1588 cm^{-1} (G-band) and 1379 cm^{-1} (D-band) are assigned to the stretching C=C backbone and antisymmetric stretching of C-N bond in PPy-NTs, respectively (Fig. 2a). In addition, the smaller intensity of D-band as compared to G-band (I_D/I_G=0.92) is related to the less defects present in PPy-NTs [14]. Moreover, the peak at 1269 cm^{-1} is assigned to the C-H in-plane and the ring stretching while the peaks at 978 and 1040 cm^{-1} associated with polaron and peak at 1070 cm^{-1} indicates the bipolaron structure. The ring deformation vibration is assigned by the peak at 919 cm^{-2} [9]. Impressively, it is obvious that N-CNTs exhibited two peaks at around 1355 and 1571 cm^{-1} (Fig. 2b). The former peak originates from disorder-induced amorphous carbon (D band) due to the finite particle size effect, lattice distortion, and/or the presence of structural defects. On the other hand, the latter peak (G band) is assigned to graphite since the shift of highly

oriented pyrolytic graphite is found at 1572 cm^{-1}. The relative intensity of G band with respect to D band (I_G/I_D), therefore, indicates the degree of N-CNT purity, which depends on the crystal planar domain size of graphite. It has been estimated that I_G/I_D for N-CNTs is found to be 0.96, suggesting high purity of CNTs [15]. It further noticed that, the value of I_D/I_G for N-CNTs is higher than that for PPy-NTs, indicating presence of more defects and active sites which can be ascribed to the doped nitrogen.

Fig. 3 shows SEM images of PPy-NTs and N-CNTs with corresponding EDS patterns. As seen in Fig. 3 (a), PPy-NTs are randomly spread with well-developed nanoscale pores. No aggregation and alignment of bundles of PPy-NTs has been observed. The EDS analysis of PPy-NTs suggests the presence of C, N, O and Cl, confirming the formation Cl doped PPy nanostructure (Fig. 3 (b)). Inclusion of oxygen may correspond to the surface oxidation of PPy-NTs. It is further interesting to note that, high carbonization temperature (800 ºC) does not change the original 1D nanostructure of PPy-NTs (Supporting information S1). Also, the tubes are of few micrometer in length and nanometer in diameter (Fig. 3 (c)). However, considerable difference in EDS spectrum of N-CNTs has been observed. The intensities of C and N peaks are considerably increased while that of O peak is decreased and Cl is completely removed, suggesting higher percentage of C and N as compared to PPy-NTs sample. Such 1D nanostructured PPy-NTs and N-CNTs are highly useful in energy storage devices, particularly in supercapacitors. In order to get more insights about the size and shape of the samples, STEM analysis has been carried out and shown in Fig. 3 (e, f). The PPy-NTs exhibits outer and inner diameters of about 170-190 nm and 80-100 nm, respectively which slightly decreased to 120-140 and 50-70 for N-CNTs (Fig. 3 f). In addition, the outer surface of N-CNTs samples looks more amorphous due to high temperature treatment as clearly observed in STEM images (Fig. 3 e, f). The small diameter nanotubes of both samples, PPy-NTs and N-CNTs can give rise to many interesting electronic properties such as high electrochemically active surface area, easy

access for electrolytic ions for transportation which is beneficial to supercapacitors application (Supporting information S2).

It is generally known that the BET surface area and pore-size distributions are directly correlated to the specific capacitance [16]. Surface area and pore-size distribution analysis of PPy-NTs and N-CNTs were conducted using N_2 adsorption and desorption experiments and presented in Fig. 4 (a, b). As seen from Fig. 4 (a), the profile of the hysteresis loop indicates an adsorption-desorption characteristics of the porous materials. The BET specific surface areas of the PPy-NTs and N-CNTs materials obtained were 43.5 and 58.9 m^2g^{-1}, respectively which is considerably higher than other PPy nanostructures [17]. Interestingly, the BET specific surface area of N-CNTs is higher than that of the pure PPy-NTs which may be attributed to the formation of amorphous graphitic texture after carbonization. The BJH pore size distributions of PPy-NTs and N-CNTs samples are calculated using the desorption curve. The curves in Fig. 4 (b) for both samples reveal the presence of hierarchically porosity: <2 nm micropores, 4 nm mesopores and 20-100 nm macro/mesopores. It is easy to conclude that the micropores located within the mesopore nanotubular walls which can provide the electric-double-layer capacitance. The N-CNTs sample shows higher mesoporosity as exhibits relatively high intense peak at around 4 nm. It can provide low-resistant pathways for the ions through the porous structure, as well as a shorter diffusion route because of the ordered mesoporous channels. The larger mesoporous structure (20-50 nm) is a consequence of the porous nanotubes. Maintaining such a macro/mesoporous structure can potentially offer enhanced electrolyte access to the high interfacial areas which may improve the charge transport and power capability. Meanwhile, ion-buffering reservoirs formed in the larger mesopores can reduce the diffusion distances to the interior surfaces [18].

Electrochemical studies

The electrochemical features of PPy-NTs and N-CNTs electrodes are studied using cyclic voltammetry (CV) and galvanostatic charge-discharge (GCD) measurement in 1 M H_2SO_4 electrolyte. Fig. 5 (a) shows the CV curves of PPy-NTs at various scan rates (5-100 mV/s) within potential window of 0-0.9 V (vs, Ag/AgCl). The CV curves show obvious well-defined redox peaks for PPy-NTs electrodes, suggesting the main capacitive contribution from pseudo-capacitance of PPy. The current under the curve slowly increases with scan rate. It should also be noted that as the scan rate is increased, the potential of the anodic and cathodic peaks shift slightly in the more positive and negative directions, respectively. This shows that the voltammetric currents are directly proportional to the scan rate and thereby display capacitive behavior [19]. It is worth noting that, the shape of CV curves remains unchanged as the scan rate increases from 5 to 100 mV/s, demonstrating the excellent capacitive behavior and high-rate capability. Further to study the rate capability of PPy-NTs electrode, the GCD is performed at various current densities (1-20 mA/cm^2) presented in Fig. 5 (b). The non-triangular GCD shapes further confirms the inclusion of pseudo-capacitive behavior of PPy-NTs electrode which supports to the CV results. Moreover, the small internal resistance (*iR*) drop for PPy-NTs electrode may be attributed to the mesopores nanotubular structure of PPy-NTs which allows fast ion transportation during charge/discharge cycle. Fig. 5 (c) shows the CV curves of N-CNTs electrode at various scan rates (5-100 mV/s) within potential window of +0.3 to -0.5 V (vs, Ag/AgCl) in 1 M H_2SO_4 electrolyte. It is interesting to reveal that, the shapes of CV curves are far different than PPy-NTs, exhibits symmetric nature along anodic and cathodic direction without any obvious redox peaks. These finding suggests the dominating electric double layer capacitive (EDLC) behavior of N-CNTs. Moreover, it is seen that the curves are not ideal rectangular suggesting the faradaic contribution from foreign dopant (nitrogen) in CNTs. The specific capacitances of PPy-NTs and N-CNTs electrodes are derived from the discharging curves using following equation,

$$C_s = \frac{I_d \times T_d}{\Delta V \times m} \quad (1)$$

where, C_s is specific capacitance, I_d is discharge current, T_d is the discharge time, ΔV is potential window, and m is the mass of active material. For PPy-NTs and N-CNTs electrodes, the mass of active material were 0.8 and 1.1 mg/cm, respectively. The maximum specific capacitance of 332 and 228 F/g is obtained at current density 1 mA/cm for PPy-NTs and N-CNTs electrode, respectively. Fig. 5 (d) shows the variation of specific capacitances of PPy-NTs and N-CNTs with current density. It is observed that the specific capacitance decreases with current density which is attributed to less utilization of electroactive material at high current densities [20].

Another aspect which must be considered is the fabrication of supercapacitors with high energy density which is possible by extending their operational voltage window (since, $E=0.5 CV^2$). In this sense, construction of asymmetric capacitors with pseudo-capacitive material cathodes and EDLC anodes in aqueous electrolytes is the most frequently adopted pathway [21]. Here, we have assembled asymmetric capacitors with PPy-NTs as a positive and N-CNTs as a negative electrode with 1 M H_2SO_4 electrolyte. In this asymmetric device, PPy-NTs stored the charges by redox reactions while the N-CNT stores the charges by non-faradic mechanism. In order to get higher cell voltage, the mass loading of both the electrodes must be adjusted to balance the stored charges. The optimized mass ratio from positive to negative electrode is 0.7: 1. Hence we adjust the mass of PPy-NTs and N-CNT to 0.29 and 0.41 mg/cm^2, respectively.

Taking advantage of different operating potential of PPy-NTs and N-CNTs electrodes in 1 M H_2SO_4 (Fig. 6 (a)), it is anticipated that the operating potential of cell can be extended up to 1.4 V when they are assembled into asymmetric design. Fig. 6 (b) shows the CV curves of PPy-NTs//N-CNTs asymmetric cell at various scan rates (5-100 mV/s) within operating potential

window of 0 to 1.4 V. The CV curve demonstrates symmetric nature along cathodic and anodic direction indicating better capacitive behavior of PPy-NTs//N-CNTs asymmetric cell. Moreover, the current density increases with the scan rate. Even at high scan rate of 100 mV/s, CV curve maintains their original shape indicating the high rate capability of PPy-NTs//N-CNTs asymmetric cell. The GCD curves of PPy-NTs//N-CNTs asymmetric cell at various current densities is presented in Fig. 6 (c). The decrease in charge-discharge time with increasing current density is due to the diffusion limits in charge transport at higher current density. Therefore, the specific capacitance of PPy-NTs//N-CNTs asymmetric cell decreases with current density (Fig. 7 (d)). The maximum specific capacitance of 109 F/g (1.57 F/cm^3) is obtained at current density of 1.43 A/g. This value is considerably higher than the values reported for other asymmetric cells (Supporting information S4) [22]

The energy density (E) and power density (P) are two important parameters as far as concern with the energy storage devices, therefore we calculate the E and P at various current density and plotted in Ragone plot (Fig. 7 (a, b)). The maximum energy density of PPy-NTs//N-CNTs cell is found to be 28.98 Wh/kg (0.4 mWh/cm^3) at power density of 998.56 W/kg (14 mW/cm^3). More interestingly, even at high power density of 7.75 kW/kg (113.4 mW/cm^3), PPy-NTs//N-CNTs exhibits energy density of 6.88 Wh/kg (0.09 mWh/cm^3), confirming the promising application in high performance devices. The energy density demonstrated in this work is significantly higher than those obtained for other carbon-based symmetric capacitors in aqueous electrolytes, such as activated carbon (<10 Wh/kg) [23], carbon nanotubes (<10 Wh/kg) [24], graphene (9.1 Wh/kg) [25]. The excellent performance is also comparable or superior to other asymmetric cells with mild aqueous electrolytes [5b, 21b, 26, 27]. For instance SnO_2//PPy-MnO_2 (27.2 Wh/kg) [28], MWNTs-NiO//MWNTs (3.8 Wh/kg) [29], $Co(OH)_2$//GO (11.94 Wh/kg) [30]. Further, the galvanostatic charge/discharge cycling performance was tested at different current

densities for 2000 cycles. Impressively, PPy-NTs//N-CNTs cell found to be stable, with cycle retention of 89.9 % after 2000 charge/discharge cycles (Fig. 7 c). Nyquist plot of PPy-NTs//N-CNTs cell within a frequency range of 1 KHz to 0.1 mHz as seen in Fig. 7 (d). The impedance plot shows very small equivalent series resistance of 1.65 Ωcm^{-2} and charge transfer resistance of 0.10 Ωcm^{-2}. These all excellent electrochemical properties are attributed to the following aspects: (1) nanotubular shape offers direct current pathway as well as very short ion diffusion lengths, (2) additionally; nanotubes provide high surface area, enabling large electrolyte-electrode contact area and reducing the charge-discharge time (3) furthermore, nanotubes restrain the mechanical degradation, enabling long-life cycling.

Conclusion

In summary, we have successfully implemented a novel approach to fabricate asymmetric capacitor in which polypyrrole nanotubes (PPy-NTs) are used as positive and N-doped carbon nanotubes (N-CNTs) (carbonized PPy-NTs) as negative electrodes. Highly porous PPy-NTs and enormous graphitic texture with copious heteroatom functionalities, N-CNTs demonstrates high single-electrode capacitance over 332 $F/g_{(PPy\text{-}NTs)}$ and 228 $F/g_{(N\text{-}CNTs)}$ in 1 M H_2SO_4 aqueous solution. Further, PPy-NTs//N-CNTs asymmetric cell effectively provides high operation voltage (1.4 V) and hence high energy density over 28.95 Wh/kg (0.41 mWh/cm^3) with a high power density of 7.75 kW/kg (113 mW/cm^3) and cyclic stability of 89.98 % after 2000 cycles. This novel synthesis approach might be useful to develop the high energy density supercapacitors, which can be applicable for various portable electronic devices.

Acknowledgements

Authors appreciate the award to DPD with the support of the Secretary for Universities and Research of the Ministry of Economy and Knowledge of the Government of Catalonia and

the Co-fund programme of the Marie Curie Actions of the 7th R&D Framework Programme of the European Union". ICN2 acknowledges support of the Spanish MINECO through the Severo Ochoa Centers of Excellence Program under Grant SEV-2013-0295. And CAPES Foundation, Ministry of Education of Brazil: Process BEX 3196/14-3.

References

[1] (a) D. P. Dubal, O. Ayyad, V. Ruiz, P. Gomez-Romero, *Chem. Soc. Rev.,* 2015, **44,** 1777, (b) J. R. Miller, P. Simon, *Science*, 2008, **321**, 651. (c) J. M. Tarascon, M. Armand, *Nature*, 2001, **414**, 359

[2] (a) C. D. Lokhande, D. P. Dubal, O. S. Joo, *Curr. Appl. Phys.,* 2011, **11**, 255. (b) J. Suárez-Guevara, V. Ruiz, P. Gomez-Romero, *J. Mater. Chem. A*, 2014, **2**, 1014. (c) I. Shown, A. Ganguly, L. C. Chen, K. H. Chen *Energy Science and Engineering,* 2015, **3**, 2

[3] Z. Yu, L. Tetard, L. Zhai, J. Thomas, *Energy Environ. Sci.*, 2015, **8**, 702

[4] D. P. Dubal, P. Gomez-Romero, B. R. Sankapal, R. Holze, *Nano Energy,* 2015, **11**, 377

[5] (a) T. Zhai, X. Lu, Y. Ling, M. Yu, G. Wang, T. Liu, C. Liang, Y. Tong, Y. Li, *Adv. Mater.* 2014, **26**, 5869. (b) X. Lu, Y. Zeng, M. Yu, T. Zhai, C. Liang, S. Xie, M. S. Balogun, Y. Tong, *Adv. Mater.* 2014, **26**, 3148

[6] F. Wang, S. Xiao, Y. Hou, C. Hu, L. Liu, Y. Wu, *RSC Adv.*, 2013, **3**, 13059

[7] (a) J. Ji, L. L. Zhang, H. Ji, Y. Li, X. Zhao, X. Bai, X. Fan, F. Zhang, R. S. Ruoff, *ACS Nano* 2013, **7**, 6237. (b) H. Chen, L. Hu, Y. Yan, R. Che, M. Chen, L. Wu, *Adv. Energy Mater*., 2013, **3**, 1636

[8] (a) J. Wei, D. Zhou, Z. Sun, Y. Deng, Y. Xia, D. Zhao, *Adv. Funct. Mater.,* 2013, **23**, 2322. (b) Z. Li, Z. W. Xu, X. H. Tan, H. L. Wang, C. M. B. Holt, T. Stephenson, B. C. Olsen, D. Mitlin, *Energy Environ. Sci.*,2013, **6**, 871

[9] N. Su, H. B. Li, S. J. Yuan, S. P. Yi, E. Q. Yin, *eXPRESS Polymer Letters,* 2012, **6**, 697

[10] D. P. Dubal, S. H. Lee, J. G. Kim, W. B. Kim, C. D. Lokhande, *J. Mater. Chem.*, 2012, **22**, 3044.

[11] G. C. Marjanovi, I. Pašti, N. Gavrilov, A. Janoševi, S. Mentus, *Chemical Papers* 2013, **67**, 781

[12] H. Ago, T. Kugler, F. Cacialli, W. R. Salaneck, M. S. P. Shaffer, A. H. Windle, R. H.

Friend, *J Phys Chem B* 1999, **103**, 8116

[13] (a) H. K. Jeong, Y. P. Lee, Rob J. W. E. Lahaye, M. H. Park, K. H. An, I. J. Kim, C. W. Yang, C. Y. Park, R. S. Ruoff, Y. H. Lee, *J. Am. Chem. Soc.*, 2008, **130**, 1362. (b) Z. H. Sheng, L. Shao, J. J. Chen, W. J. Bao, F. B. Wang, X. H. Xia, *ACS nano* 2011, **5**, 4350

[14] B. Xu, H. Duan, M. Chu, G. Cao, Y. Yang, *J. Mater. Chem. A,* 2013, **1**, 4565-70

[15] S. S. Islam, K. A. Shah, H. S. Mavi, A. K. Shukla, S. Rath, Harsh *Bull. Mater. Sci.* 2007, **30**, 295

[16] (a) H. Jiang, J. Ma, C. Li, *Chem. Commun.*, 2012, **48**, 4465. (b) C. Yuan, J. Li, L. Hou, L. Yang, L. Shen, X. Zhang, *J. Mater. Chem.*, 2012, **22**, 16084

[17] (a) M. Sharma, G. I. N. Waterhouse, S. W. C. Loader, S. Garg, D. Svirskis, *Inter. J. Pharma.* 2013, **443**, 163. (b) Y. Li, K. G. Neoh, L. Cen, E. T. Kang, *Langmuir,* 2005, **21**, 10702. (c) B. Veeraraghavan, J. Paul, B. Haran, B. Popov, *J. Power Sources*, 2002, **109**, 377

[18] J. Zhang, L. B. Kong, J. J. Cai, H. Li, Y. C. Luo, L. Kang *Microporous Mesoporous Mater.* 2010, **132**, 154

[19] D. P. Dubal, R. Holze, P. Gomez-Romero, *Sci. Rep.* 2014, **4**, 7349

[20] (a) J. Li, X. Cheng, J. Sun, C. Brand, A. Shashurin, M. Reeves, M. Keidar, *J. Appl. Phys.* 2014, **115**, 164301. (b) N. R. Chodankar, D. P. Dubal, G. S. Gund, C. D. Lokhande, *Electrochim. Acta* 2015, **165**, 338

[21] (a) J. A. Stasera, J. W. Weidner, *J. Electrochem. Soc.*, 2014, **161**, E3267. (b) P. Yang, Y. Ding, Z. Lin, Z. Chen, Y. Li, P. Qiang, M. Ebrahimi, W. Mai, C. P. Wong, Z. L. Wang, *NanoLett.* 2014, **14**, 731

[22] (a) D. P. Dubal, N. R. Chodankar, G. S. Gund, R. Holze, C. D. Lokhande, P. Gomez-Romero, *Energy Technol.* 2015, **3**, 168. (b) R. R. Salunkhe, H. Ahn, J. H. Kim, Y. Yamauchi, *Nanotechnology,* 2015, **26***,* 204004. (c) J. Huang, P. Xu, D. Cao, X. Zhou, S.

Yang, Y. Li, G. Wang *J. Power Sources,* 2014, **246**, 371

[23] D. W. Wang, F. Li, M. Liu, G. Q. Lu, H. M. Cheng, *Ang. Chem. International Ed.*, 2008, **47**, 373-6

[24] C. Yu, C. Masarapu, J. Rong, B. Wei, H. Jiang, *Adv. Mater.*, 2009, **21**, 4793

[25] H. Wang, Y. Liang, T. Mirfakhrai, Z. Chen, H. S. Casalongue, H. Dai *Nano Res.*, 2011, **4**, 729

[26] X. Lu, M. Yu, G. Wang, T. Zhai, S. Xie, Y. Ling, Y. Tong, Y. Li, *Adv. Mater.* 2013, **25**, 267

[27] W. Zilong, Z. Zhu, J. Qiu, S Yang, *J. Mater. Chem. C,* 2014, **2**, 1331

[28] F. Grote, Y. Lei, *Nano Energy*, 2014, **10**, 63

[29] A S Adekunle, K I Ozoemena, B B Mamba, B O Agboola, O S Oluwatobi, *Int. J. Electrochem. Sci.,* 2011, **6**, 4760

[30] R R Salunkhe, B P Bastakoti, C T Hsu, N Suzuki, J H Kim, S X Dou, C C Hu, Y. Yamauchi, *Chem. Eur. J.*, 2014, **20**, 3084

Figure Caption

Fig. 1 (a) XRD patterns of PPy-NTs and N-CNTs samples, (b) Full XPS survey spectrum of PPy-NTs and N-CNT (c) core-level C1s spectrum for N-CNTs and (d) Magnified N1s spectra for PPy-NTs and N-CNT samples.

Fig. 2 Raman spectra for (a) PPy-NTs and (b) N-CNTs samples

Fig. 3 (a-c) FE-SEM, EDAX and STEM images of PPy-NTs samples, respectively and (d-f) FE-SEM, EDAX and STEM images of N-CNTs samples, respectively

Fig. 4 Nitrogen adsorption/desorption isotherm of PPy-NTs and N-CNTs (a) with corresponding pore size distribution curves (b).

Fig. 5 (a) CV curves of PPy-NTs electrode at various scan rate from 5-100 mV/s (b) Galvanostatic charge/discharge curves of PPy-NTs at current densities (c) CV curves of N-CNTs at various scan rate from 5-100 mV/s (d) Plot of specific capacitance versus current density for PPy-NTs and CNTs electrodes

Fig. 6 (a) CV curves of PPy-NTs and N-CNTs within different operating potential window in 1 M H_2SO_4 electrolyte at constant scan rate of 10 mV/s (b) CV curves of PPy-NTs//N-CNTs asymmetric cell within operating voltage window of 1.4 V at various scan rates (c) Galvanostatic charge/discharge curves of PPy-NTs//N-CNTs asymmetric cell at different current densities (d) Plot of specific capacitance versus current density for PPy-NTs//N-CNTs asymmetric cell

Fig. 7 (a, b) Plots of energy density versus power density of PPy-NTs//N-CNTs asymmetric cell in Ragone plot, (c) Variation of specific capacitance with number of cycles measured at different current densities, (d) Nyquist plot of PPy-NTs//N-CNTs cell within a frequency range of 1 KHz to 0.1 mHz

Figure(s)

Click here to download Figure(s): Figures.doc

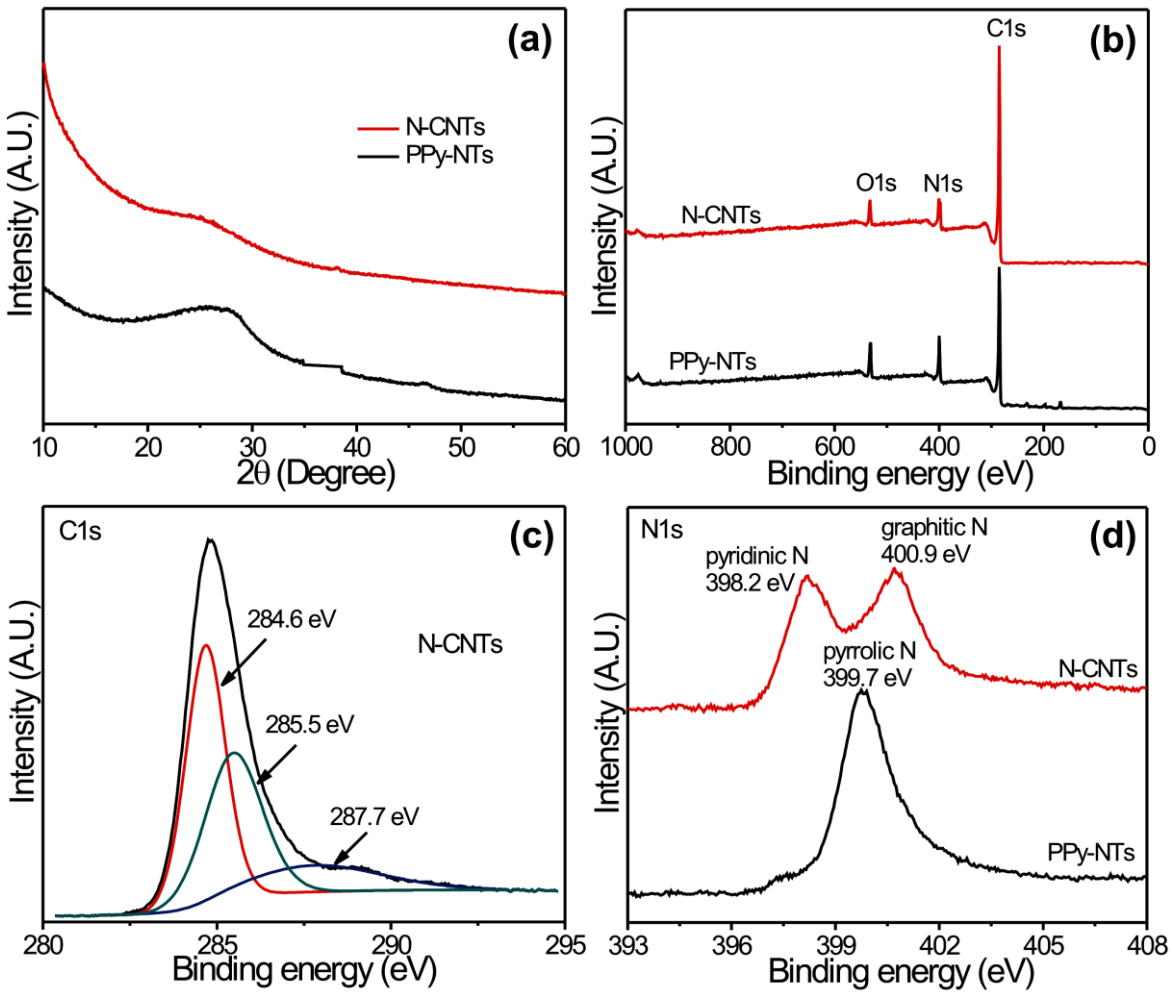

Fig. 1

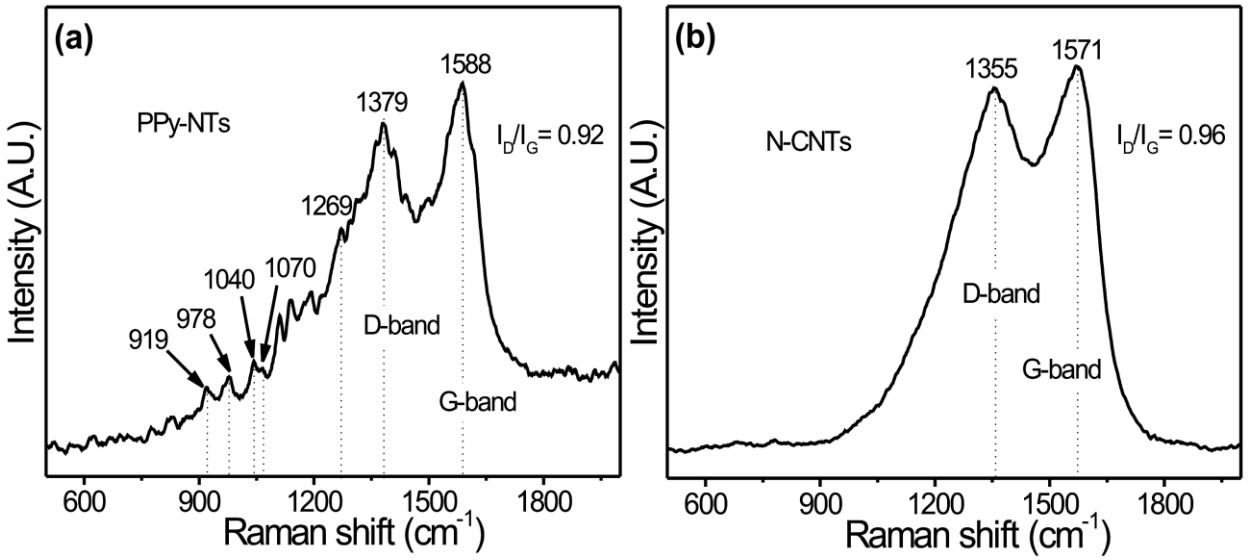
(a)
PPy-NTs
I_D/I_G= 0.92
1588
1379
1269
1070
1040
978
919
D-band
G-band
Intensity (A.U.)
600
900
1200
1500
1800
Raman shift (cm^{-1})
(b)
N-CNTs
I_D/I_G= 0.96
1571
1355
D-band
G-band
Intensity (A.U.)
600
900
1200
1500
1800
Raman shift (cm^{-1})

Fig. 2

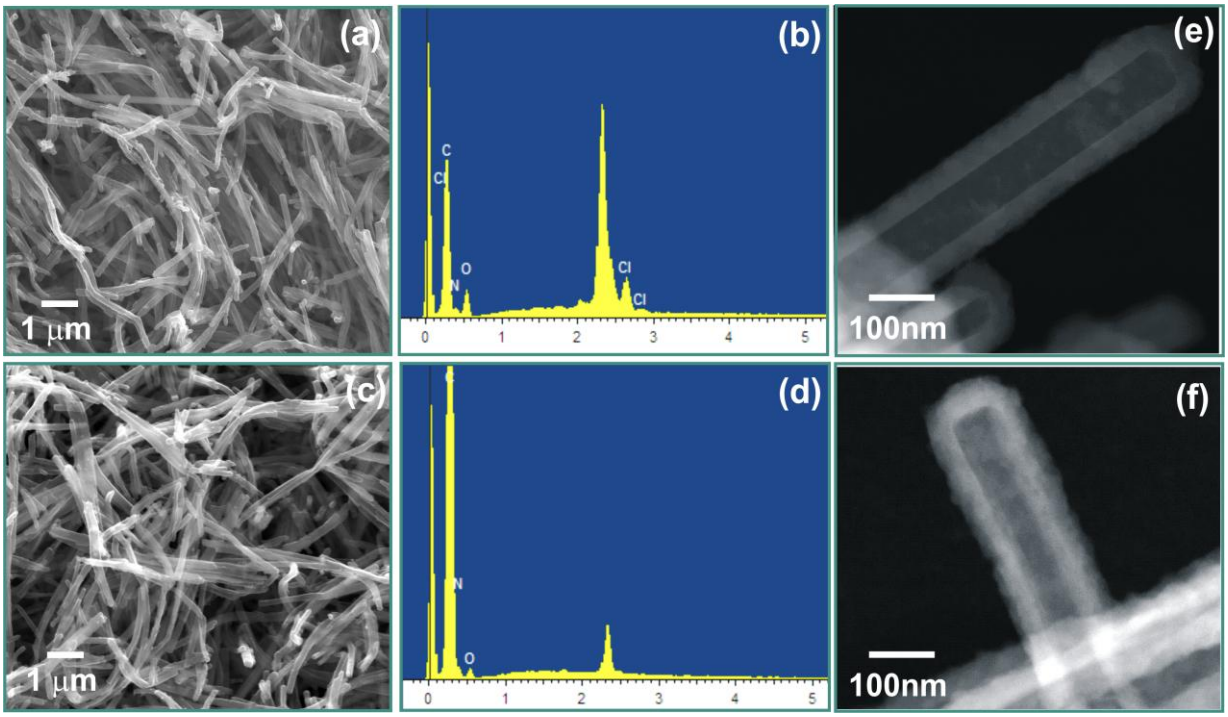

Fig. 3

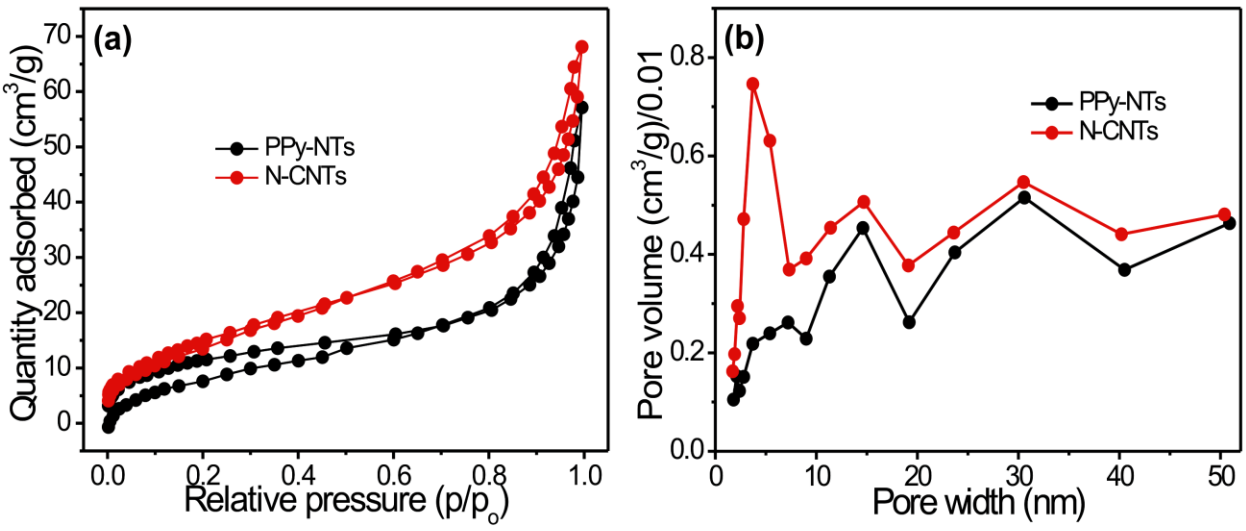
(a)
Quantity adsorbed (cm3/g)
Relative pressure (p/po)
PPy-NTs
N-CNTs
(b)
Pore volume (cm3/g)/0.01
Pore width (nm)
PPy-NTs
N-CNTs

Fig. 4

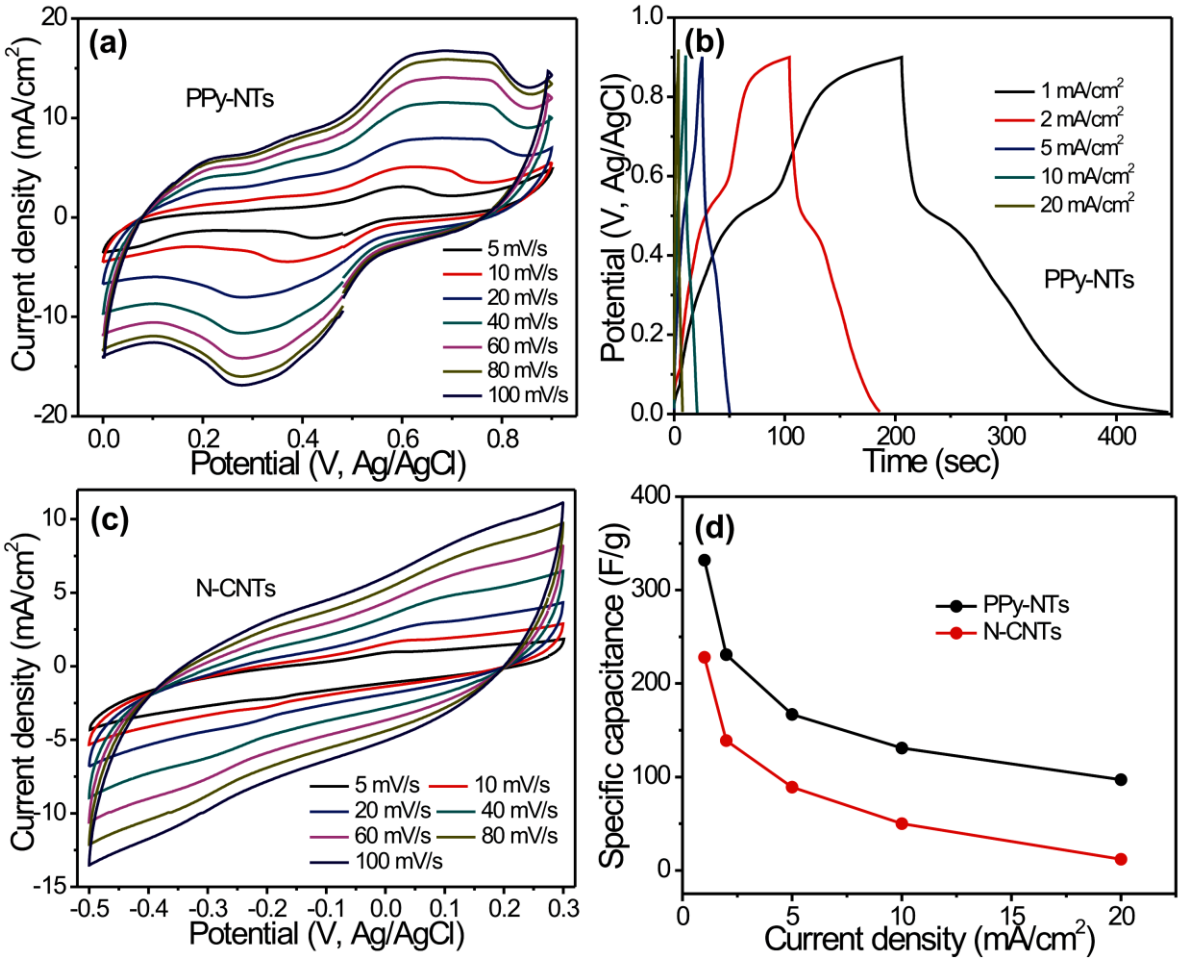
(a)
PPy-NTs
Current density (mA/cm²)
Potential (V, Ag/AgCl)
5 mV/s
10 mV/s
20 mV/s
40 mV/s
60 mV/s
80 mV/s
100 mV/s
(b)
Potential (V, Ag/AgCl)
Time (sec)
1 mA/cm²
2 mA/cm²
5 mA/cm²
10 mA/cm²
20 mA/cm²
PPy-NTs
(c)
N-CNTs
Current density (mA/cm²)
Potential (V, Ag/AgCl)
5 mV/s
10 mV/s
20 mV/s
40 mV/s
60 mV/s
80 mV/s
100 mV/s
(d)
Specific capacitance (F/g)
Current density (mA/cm²)
PPy-NTs
N-CNTs

Fig. 5

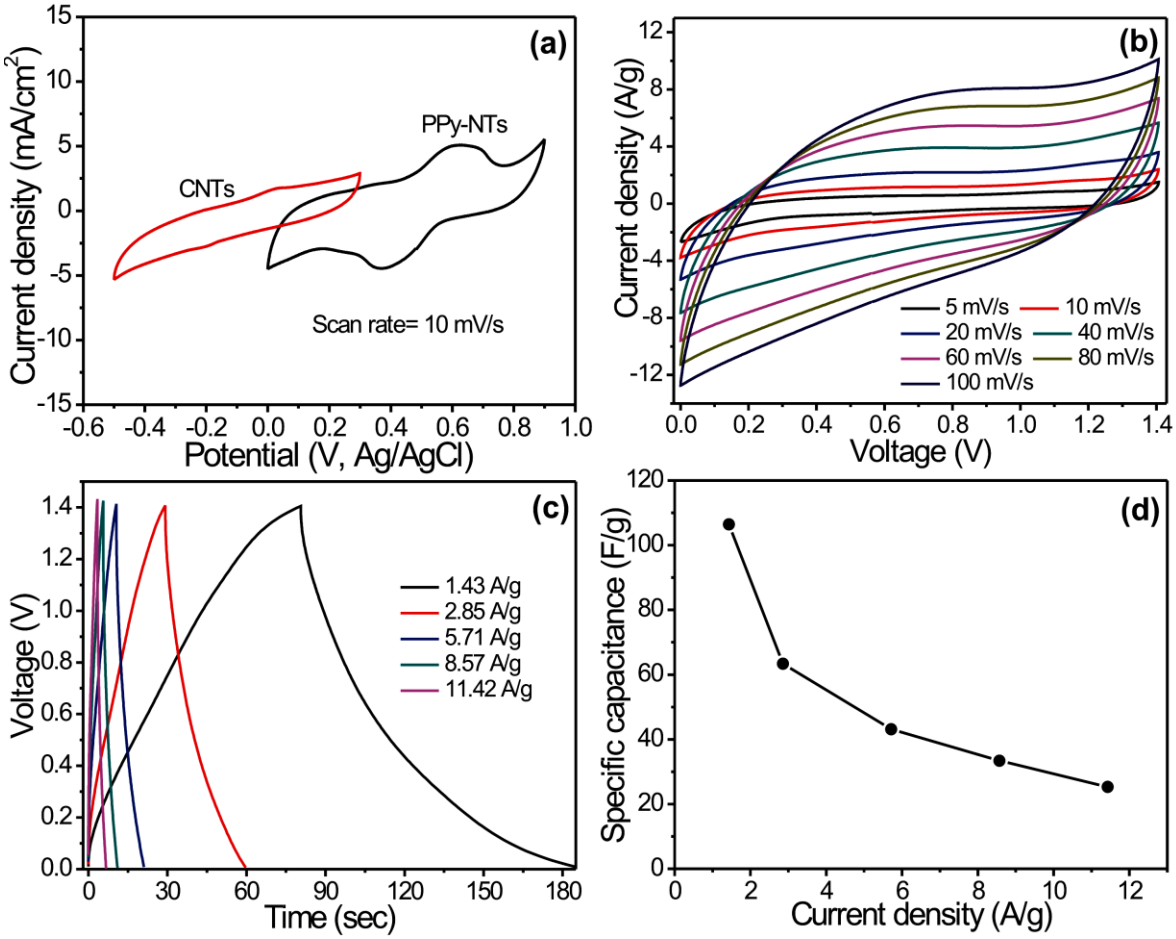
(a)
Current density (mA/cm^2)
Potential (V, Ag/AgCl)
CNTs
PPy-NTs
Scan rate= 10 mV/s
(b)
Current density (A/g)
Voltage (V)
5 mV/s
10 mV/s
20 mV/s
40 mV/s
60 mV/s
80 mV/s
100 mV/s
(c)
Voltage (V)
Time (sec)
1.43 A/g
2.85 A/g
5.71 A/g
8.57 A/g
11.42 A/g
(d)
Specific capacitance (F/g)
Current density (A/g)

Fig. 6

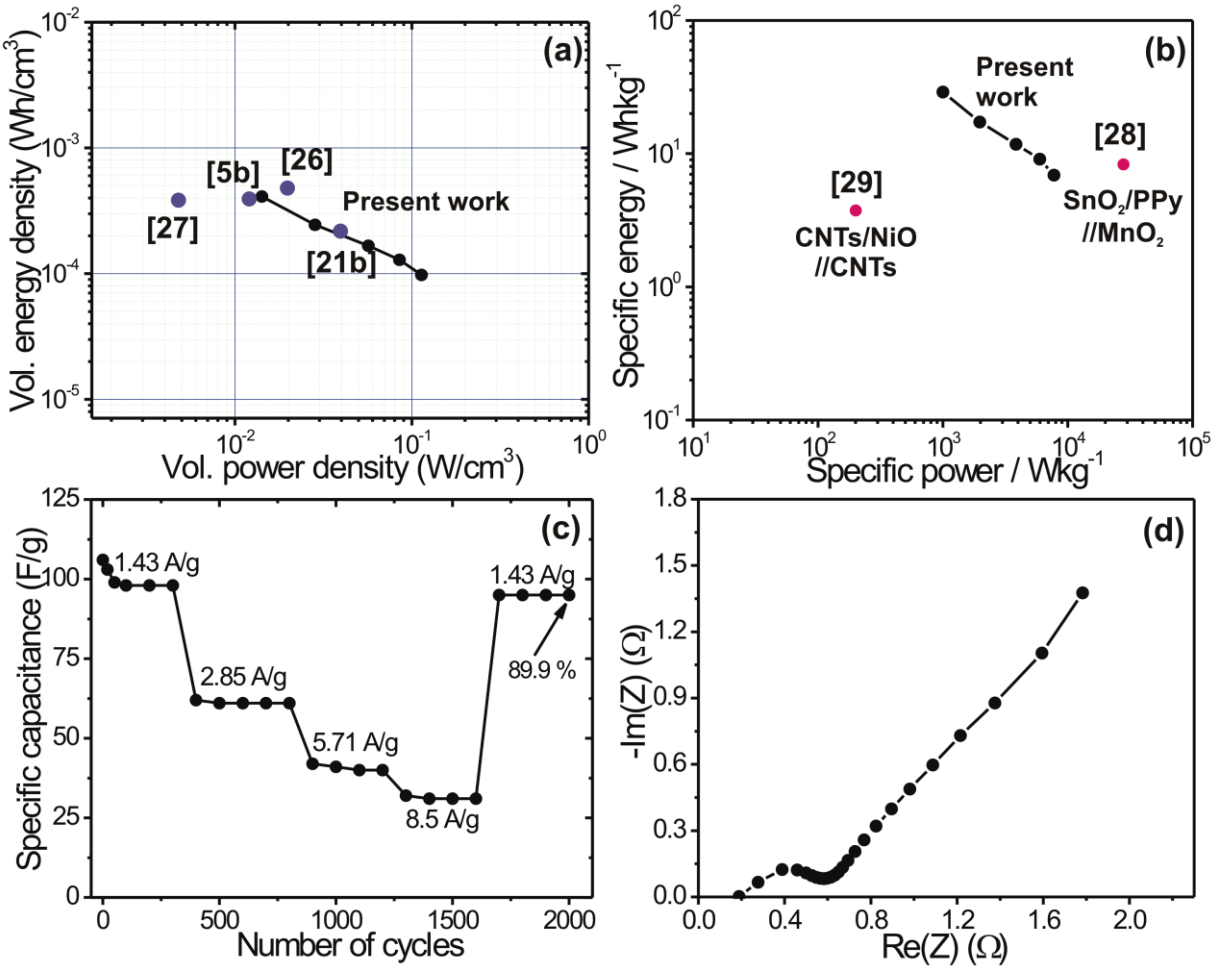
(a)
Vol. energy density (Wh/cm3)
Vol. power density (W/cm3)
[27]
[5b]
[26]
Present work
[21b]
(b)
Specific energy / Whkg-1
Specific power / Wkg-1
Present work
[28]
[29]
SnO2/PPy //MnO2
CNTs/NiO //CNTs
(c)
Specific capacitance (F/g)
Number of cycles
1.43 A/g
2.85 A/g
5.71 A/g
8.5 A/g
1.43 A/g
89.9 %
(d)
-Im(Z) (Ω)
Re(Z) (Ω)

Fig. 7

Supplementary Materials

Click here to download Supplementary Materials: Supporting information.doc